Article

Journal of Tissue Engineering
4: 2041731413518060

DOI: 10.1177/2041731413518060
tej.sagepub.com
SAGE

Porcine cholecyst–derived scaffold promotes full-thickness wound healing in rabbit

Deepa Revi, Vadavanath Prabhakaran Vineetha, Jaseer Muhamed, Akhila Rajan, and Thapasimuthu Vijayamma Anilkumar

Abstract
Graft-assisted healing is an important strategy for treating full-thickness skin wounds. This study evaluated the properties of porcine cholecyst–derived scaffold and its use for treating full-thickness skin wound in rabbit. The physical properties of cholecyst-derived scaffold were congenial for skin-graft application. Compared to a commercially available skin-graft substitute made of porcine small intestinal submucosa, the cholecyst-derived scaffold was rich in natural biomolecules like elastin and glycosaminoglycans. When used as a xenograft, it promoted healing with excess cell proliferation at early phases and acceptable collagen deposition in the later remodelling phases.

Keywords
Wound healing, cholecyst-derived scaffold, graft-assisted healing, skin graft, extracellular matrix, collagen

Received: 18 November 2013; accepted: 27 November 2013

Introduction

The use of acellular scaffolds of xenogenic origin, essentially extracellular matrices of various organs/tissues resulting after removal of cells, as skin substitute is an acceptable modality for treating dermal wounds but there are several drawbacks for such graft-assisted healing strategies.[1] Most of these problems are associated with defective healing process caused by 'healing by repair' that causes excess scar tissue formation. Ideally, restoration of a fully functional skin is desired,[2] but this is often restricted to 'healing by regeneration' that favours the replacement of epithelial (epidermal) cells. Excess collagen deposition may complicate the healing reaction. Therefore, those acellular grafts that aid healing by regeneration and optimal deposition of collagen are preferred over those promoting scarring for clinical use. Furthermore, it should also create a microenvironment favourable for migration and infiltration of various cells such as keratinocytes, fibroblasts, endothelial cells and immune cells which contribute to the complex process of wound healing and remodelling. It is obvious that a scaffold mimicking the extracellular matrix (ECM) with adequate bioactive molecules, capable of supporting the growth of cells participating in regeneration, is an ideal graft suitable for wound healing application.[3] Indeed, ECM isolated from certain mammalian organs and tissues have been found to have these essential bio-components that support cell proliferation, migration and differentiation.[4] These scaffolds are naturally rich in collagen, elastin, glycosaminoglycans (GAGs), laminin and fibronectin on which the cells can migrate, attach and grow. In addition, many of the bioactive degradation products released from the graft at the site of the grafting mimic growth factors required for healing.[4,5] ECM is also known to aid angiogenesis by regulating the migration, proliferation and sustenance of endothelial cells.[6] Hence, ECM is correctly termed as nature's ideal scaffold material.[7]

ECM isolated from submucosal layer of small intestine, usually from jejunum, called as small intestinal submucosa (SIS) is a popular and favourite scaffold because

Division of Experimental Pathology Biomedical Technology Wing, Sree Chitra Tirunal Institute for Medical Sciences and Technology, Trivandrum, India

Corresponding author:
TV Anilkumar, Division of Experimental Pathology, Biomedical Technology Wing, Sree Chitra Tirunal Institute for Medical Sciences and Technology, Trivandrum 695012, Kerala, India.
Email: tvanilkumar@sctimst.ac.in

of its bio-inductive property that helps in constructive remodelling of injured sites in many parts of the body, including chronic wounds such as non-healing leg ulcers.[8] Small intestine submucosa made into sponge and cross-linked with 1-ethyl-3-(3-dimethylaminopropyl)carbodiimide hydrochloride showed excellent fluid absorption capability and is associated with enhanced healing of full-thickness skin wounds in rats.[9] However, some studies also reported that the SIS have no significant beneficial effect in treating full-thickness skin wounds in dogs[10] and may elicit some adverse inflammatory response.[11] There are also reports of complications arising from the clinical use of small intestine submucosa in other regenerative medical applications.[12] Hence, there is a quest for better biological scaffolds for regenerative medical applications in general and skin-graft substitutes in particular.

Cholecyst-derived scaffold (CDS) recovered from ECM of porcine gall bladder has variable application in the field of regenerative medicine.[13] Cholecyst-derived ECM is shown to act as reinforcing buttressing staples for gastrointestinal resection and anastomotic procedures.[14] It has a micro-architecture similar to heart valves, supports proliferation of valvular endothelial and interstitial cells[15] and has ability to withstand large strain.[16] Obvious inflammatory response has not been reported following deep-tissue grafting studies in animal models.[17] Studies have also shown that properties of cholecyst-derived ECM can also be functionalised and modified using chemicals.[18,19] However, the usefulness of CDS as a potential graft for treating full-thickness skin wound has not been studied yet.

This study examines the use of CDS recovered by a non-detergent/enzymatic treatment method as skin-graft substitute for treating full-thickness skin wound and whether it has the capability to promote healing. In order to demonstrate the proof of concept, this study evaluated the wound-healing properties of CDS as a skin graft in a rabbit wound model.

Materials and methods

Scaffold preparation

CDS. ECM scaffolds for tissue engineering application were isolated from porcine gall bladder by an in-house procedure that involves mechanical recovery of lamina propria after ex situ treatment with a stabilising agent (10% buffered formalin), which resulted in controlled pre-isolation in situ cross-linking of biomolecules in the scaffold. It was washed thoroughly with water for at least 4 h, lyophilised and sterilised by ethylene oxide treatment. The resulting sheet of ECM was designated as CDS. No other detergent or enzyme treatment was performed.

Reference scaffold. Wherever indicated, one-layer tissue graft derived from SIS, marketed by Cook Surgisis® Biodesign™ was used as the reference biomaterial.

Physical properties of the grafts

Moisture content in the grafts. The specimens were cut into size of 1 cm^2, and the initial weight was noted. The samples (N = 4) were taken out, dried in an oven at 40°C for 24 h and the dried weight was noted down. Percentage of moisture content was calculated as ((initial weight − dry weight) × 100)/initial weight.

Fluid uptake. The specimens were cut into size of 1 cm^2, and the initial dry weight was noted. All the samples were soaked in phosphate-buffered saline. The samples (N = 4) were taken out, blotted and the wet weight was noted down after 1, 3, 5, 12 and 24 h. Percentage of fluid uptake was calculated as ((wet weight) − (dry weight) × 100)/(dry weight)).

Evaporative water loss. The specimens were cut into size of 1 cm^2, and the initial weight was noted. All the samples (N = 4) were soaked in water overnight, blotted and immediately weighed to get the wet weight of the scaffold. To measure evaporative water loss (EWL), the fall in weight was measured after 1, 3, 12 and 24 h and was expressed as %EWL using the formula, percentage weight remaining = ((initial weight)/(wet weight)) × 100.

Water vapour transmission rate. A 15 mL tube with 10 mL of water was sealed with the ECM scaffold, and the initial weight was noted (N = 4). The samples were placed in an incubator at 37°C for 24 h. The weight after evaporation of water from the test tube after 24 h was noted. The water vapour transmission rate (WVTR) was calculated as follows: WVTR = ((initial weight − weight after evaporation) × 10^6)/A × 24, where 'A' is the area of bottle mouth (in mm^2). The WVTR was expressed in g/mm^2/h.[20]

Young's modulus. To get the Young's modulus, the scaffolds (N = 8) were clamped at their cut ends in Universal Testing Machine (Instron Model 3365, UK). The modulus (MPa) as well as the maximum load (N) was measured using a 10 N maximum load cell with a cross-head speed of 1 mm/min, and the test was stopped when the load decreased after the onset of failure.

Flexural rigidity. The weight of 5-cm^2 rectangular scaffolds (N = 8) was measured, and the moment of inertia of the rectangular piece of the (5 cm × 1 cm) scaffolds was calculated using the formula $M = m (h^2 + w^2)/12$, where 'M' is the moment of inertia, 'm' the mass of the scaffold, 'h' is the height of the scaffold and 'w' the width of the scaffold. The moment of inertia of each scaffold calculated was multiplied with the Young's modulus of each scaffold to get the flexural rigidity of the scaffolds.[21]

Suture retention strength. The maximum load at the stress–strain curve during breakage was read as the suture retention strength (N = 8).

Biomolecule and DNA content in the scaffold

Biomolecules in the scaffold. The amount of biomolecules such as collagen, elastin and sulphated GAGs in the scaffold was estimated biochemically using Sircol collagen assay kit, Fastin elastin assay kit and Blyscan sulphated-GAGs assay kit (Bicolor Life Science Assays, UK), respectively, in both CDS and SIS using manufacturer's protocol. CHAMELEON Plate Reader with MikroWin software (Hidex, Finland) was used to measure the spectrophotometric readings.

DNA content in the scaffold. ECM scaffolds were incubated with lysis buffer 500 µL (proteinase K 20 mg/mL, 50 µL; 1M Tris-HCl solution 10 µL; 0.5M ethylenediaminetetraacetic acid (EDTA) 2 µL, 10% sodium dodecyl sulphate (SDS), 100 µL; distilled water, 838 mL) for 48 h at 60°C followed by treatment with 500µL phenol:chloroform:isopropanol alcohol at 25:24:1. The supernatant obtained after centrifugation was treated with equal volume of chloroform. Isopropanol alcohol and 3M sodium acetate (in 10:1 ratio) were added after removing the supernatant and incubated overnight at −20°C. The precipitated DNA was centrifuged at 12,000 g at 4°C and supernatant discarded. The pellet was washed in 75% ethanol, dried and was collected in 50 µL water. The DNA content was measured using nano-drop spectrophotometer.

In vivo wound healing experiment

A total of 12 healthy rabbits of more than 2 kg were randomly assigned into four groups of three each. The animal experiments were done with the approval and as per requirements of the Institutional Animal Ethics Committee. Prior to the experiment, fur on either side of the spine was clipped off. Rabbits were anaesthetised using ketamine (80 mg/kg) and xylaxin (5 mg/kg body weight). The skin of the anaesthetised rabbits were lightly swabbed using 70% alcohol and air-dried. The CDS and SIS scaffolds were grafted on full-thickness excision skin wounds of 1 cm^2 made dorsally, which were created on either side of the vertebra (N = 3). At the end of each experimental period (3, 7, 14 and 30 days), three rabbits were euthanised in a carbon dioxide chamber, and samples were collected from the wound site for histomorphology and histomorphometry evaluations.

Histomorphology and histomorphometry

After the animal experiment, the skin graft along with the surrounding normal skin was collected and fixed in 10% buffered formalin: haematoxylin and eosin staining (H&E) for routine histology, picro-sirius red staining for identifying collagen, Van Gieson staining for identifying elastin and Herovici staining for determining ratio of type I to type III collagen and for immunohistochemistry (IHC). Primary antibodies against proliferating cell nuclear antigen (PCNA; Clone PC10; Santa Cruz Biotechnologies, Inc., USA), alpha smooth muscle actin (ASMA; Clone 1A 4; Abcam, UK), vimentin (Clone V9; Dako, Denmark) and cytokeratin-14 (CK-14; Clone CKB1; Abcam, UK) were used for IHC by protocol used in this laboratory.[22]

Histomorphometry. The following wound-healing parameters were quantified by histomorphometry, wherever needed. Histology images were captured using an Olympus (BX51) microscope loaded with a DP70 camera and Image-Pro™ software. For each sample, more than six high-power fields (40X objective) were captured, and all other settings of the microscope and software were kept constant to minimise errors. The images were further evaluated with the same software as described below.

Extent of re-epithelialisation. Re-epithelialisation was quantified in images of H&E-stained sections. The length of the original wound and non re-epithelialised wound were measured, and percentage of re-epithelialisation was calculated by the formula (percentage re-epithelialisation = (length of re-epithelialised wound/length of total wound) × 100). The same was repeated for each wound site, and percentage of re-epithelialisation was determined.

Extent of collagen deposition. Images from picro-sirius red-stained sections of wound tissue were used to quantify collagen at the site of wound. The sirius red preferentially stained the collagen, and the 'red-stained' area was quantified and expressed as percentage.

Extent of angiogenesis. Images from H&E-stained sections were used to quantify angiogenesis in the vicinity of wound, and the area occupied by 'red' colour of erythrocytes was quantified and expressed as percentage angiogenesis.

Assessment of cell proliferation. This was quantified in IHC slides following staining with PCNA antibodies. The number of PCNA-positive cells in the dermis and the total number of cells in the dermis were counted in the field, and the density of proliferating cells in dermis was calculated and represented as percentage proliferation using the formula: (percentage proliferation in dermis = [(number of PCNA-positive cells in the field/total number of cells on the line) × 100].

Quantification of mesenchymal cell response. This was quantified in IHC slides following staining with vimentin antibodies. The area positive for vimentin was quantified and expressed as percentage of vimentin-stained area/high-power field.

Quantification of myofibroblast response. This was studied in IHC slides following staining with ASMA. The area

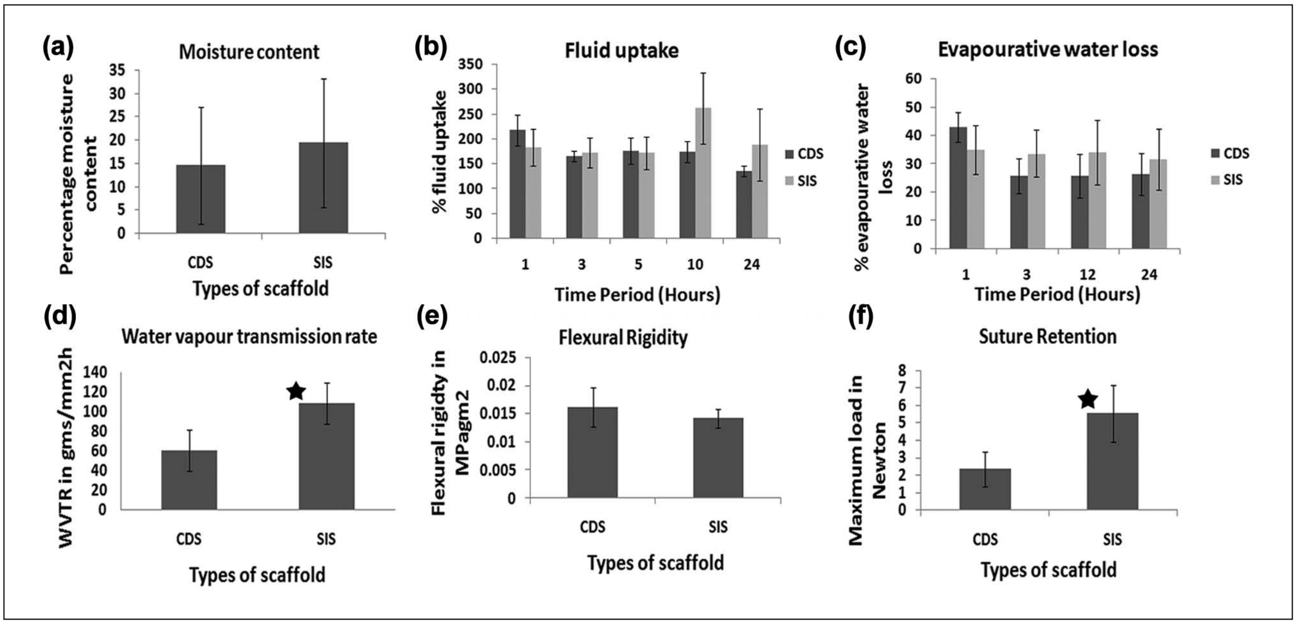

Figure 1. Physical properties of the scaffold: (a) moisture content, (b) fluid uptake, (c) evaporative water loss (EWL), (d) water vapour transmission rate (WVTR), (e) flexural rigidity and (f) suture retention strength. The CDSs have lower WVTR (p value = 0.001) and suture retention strength (p value = 0.003) than SIS.
CDS: cholecyst-derived scaffold; SIS: small intestinal submucosa.

positive for ASMA was quantified and expressed as percentage of ASMA-stained area/high-power field.

Relative distribution of type I and type III collagen. This was quantified morphometrically in Herovici-stained tissue sections.[23] With this staining procedure, the type I collagen stained red while the type III collagen stained blue in colour. Each of these was determined by area morphometry, and the ratio of type I to type III collagen was calculated.

Extent of elastin deposition. Elastin at the wound site was quantified in images of Van Gieson–stained sections of wound tissue. The elastin fibres stained black were quantified for each wound site on 7th and 30th days and were expressed as percentage of elastin.

Statistical analysis

Student's t-test was used to determine the level of significant difference between experimental groups. A p value less than 0.05 was considered to be of significance.

Results

Physical properties of the scaffold

The moisture content (Figure 1(a)), the fluid uptake (Figure 1(b)) and EWL (Figure 1(c)) in CDS were similar to that of SIS. But the WVTR (Figure 1(d)) of CDS was significantly lower (p value = 0.001) compared to SIS.

The flexural rigidity of both CDS and SIS was similar and sufficiently low as expected for a potential skin graft (Figure 1(e)), but the suture retention strength of CDS was relatively lower (p value = 0.003) compared to SIS (Figure 1(f)).

Bio-molecule and DNA content in the scaffold

The amount of collagen content was similar in CDS and SIS, but the elastin (p value = 0.0009) and GAG (p value = 0.006) contents in the CDS were significantly higher than that in SIS (Figure 2(a)). However, the DNA content in CDS was much lower (p value = 0.03) than in SIS (Figure 2(b)).

In vivo wound-healing animal experiment

The overall condition of all experimental animals remained satisfactory throughout the experiment and all the animals showed good healing response. There was no gross evidence of infection or necrosis in the retrieved wound tissue.

Histomorphology and histomorphometry

Histomorphologic signs of healing were present as early as third day and progressed to complete healing by re-epithelisation and granulation tissue formation in both CDS and SIS-grafted wounds (Figure 3). Briefly, the changes appreciated on earlier time points (3 and 7 days) were related to the

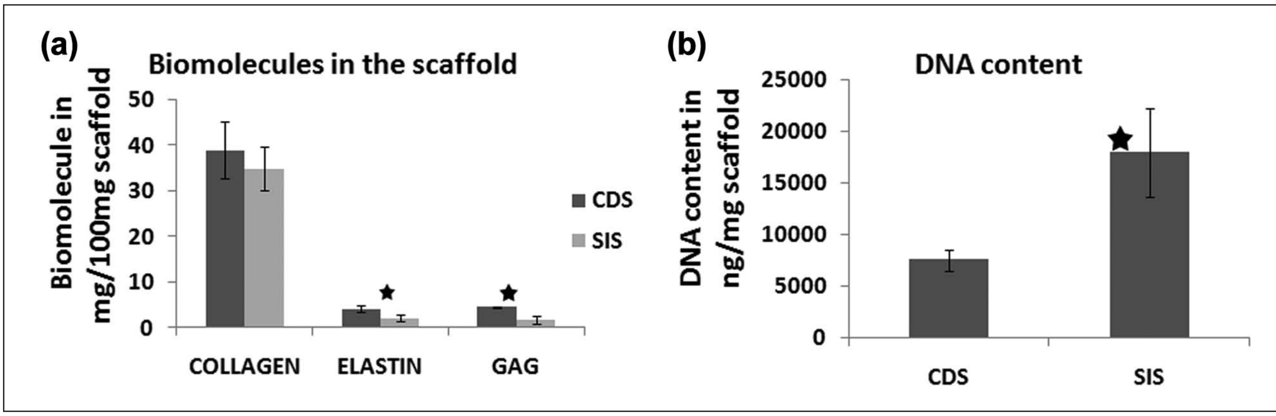

Figure 2. (a) Content of biomolecules in the candidate skin graft: the CDSs have higher elastin (p value = 0.0009) and sulphated GAG (p value = 0.006) than SIS. (b) DNA content in the scaffold: CDSs have lower DNA (p value = 0.03) compared to SIS.
CDS: cholecyst-derived scaffold; SIS: small intestinal submucosa.

proliferation (regeneration) phase, but later observations (14 and 30 days) were indicative of remodelling phase of the wound healing process. Scattered inflammatory cells were seen in histology slides made from early time points (3 and 7 days) but were minimal in later time points. The extent of cell proliferation and the process of re-epithelialisation were apparent with the abundance of PCNA-positive cells (Figure 4) and cytokeratin-positive cells in the epidermis (Figure 5). There was also an increase in the number of proliferating cells in the dermis (Figure 4), and the dermis was thickly populated by mesenchymal cells (Figure 6) and myofibroblasts (Figure 7) as identified by IHC for vimentin and ASMA intermediate filament proteins. The nature of angiogenesis (Figure 3) and collagen deposition (Figure 8) contributing for the granulation tissue formation were evident in the dermis in all phases of healing. The Herovici staining (Figure 9) and Van Gieson staining (Figure 10) reactions revealed the relative proportion and distribution of type I and type III collagen during the healing process. The quantitative data (Figures 11 and 12) were used for objective evaluation of the histomorphology results as described below.

Histomorphology with H&E staining. On the day 3, the CDS and SIS grafts were present over the healing wound tissue, but the neo-epithelium was not prominent. At this stage, the granulation tissue included only scattered collagen fibres and some newly forming blood vessels (Figure 3(a) and (b)). On the seventh day, the newly formed keratinocyte was seen in both graft-induced healing reactions, and the collagen fibres were further organised into thick bundles (Figure 3(c) and (d)). Generally, the neo-epidermis was thicker and the granulation tissue was very prominent in the dermis (Figure 3(e) and (f)). But the re-epithelialisation was not complete in all samples studied (Figure 11(a)). On the 14th day, the re-epithelialisation was almost complete and the rete pegs and ridges (arrows) of the epidermis were apparent in both groups. However, by the 30th day, there was formation of complete epidermis with prominent rete pegs and ridges. The dermis was also well developed with newly formed blood vessels and well-organised collagen fibres (Figure 3(g) and (h)). The process of remodelling was evident on these samples with reorganisation and disappearance of collagen; densely packed thick bundles were replaced by loosely placed thin strands (Figure 8). Similarly, there was no significant difference in the extent of angiogenesis between SIS and CDS; both the grafts showed similar pattern in angiogenesis (Figure 11(b)).

Extent of cell proliferation. On the third day (Figure 4(a) and (b)), most of the basal cells in the newly forming epidermis and the dermis immediately beneath were positive for PCNA. During seventh day (Figure 4(c) and (d)), both the basal and suprabasal cells in the epidermis were positive for PCNA; however, the outer layers of epidermis remained negative in all cases. By the 14th (Figure 4(e) and (f)) and the 30th day (Figure 4(g) and (h)), only basal cells in epidermis were positive for PCNA and suprabasal cells ceased to show PCNA positivity. There was increase in number of proliferating cells in CDS-grafted wound on 3rd and 14th day (Figure 11(c)).

Pattern of cytokeratin immunostaining. On the third day, keratinocytes were generally negative for CK-14 even on the leading edge of the healing wound suggestive of incomplete differentiation (Figure 5(a) and (b)). Similarly, by the seventh day, although most of the suprabasal keratinocytes of the epidermis were positive, both basal and superficial layers of epidermis showed negative for CK-14 in wounds treated by both the grafts (Figure 5(c) and (d)). Later, by 14 (Figure 5(e) and (f)) and 30 days (Figure 5(g) and (h)) of healing, the epidermis was completely formed, and CK-14 immunoreactivity was apparent in all layers of epidermis in wounds treated by both the grafts. Quantitatively (Figure 11(a)), both CDS and SIS showed 100% re-epithelisation after 14 days of grafting.

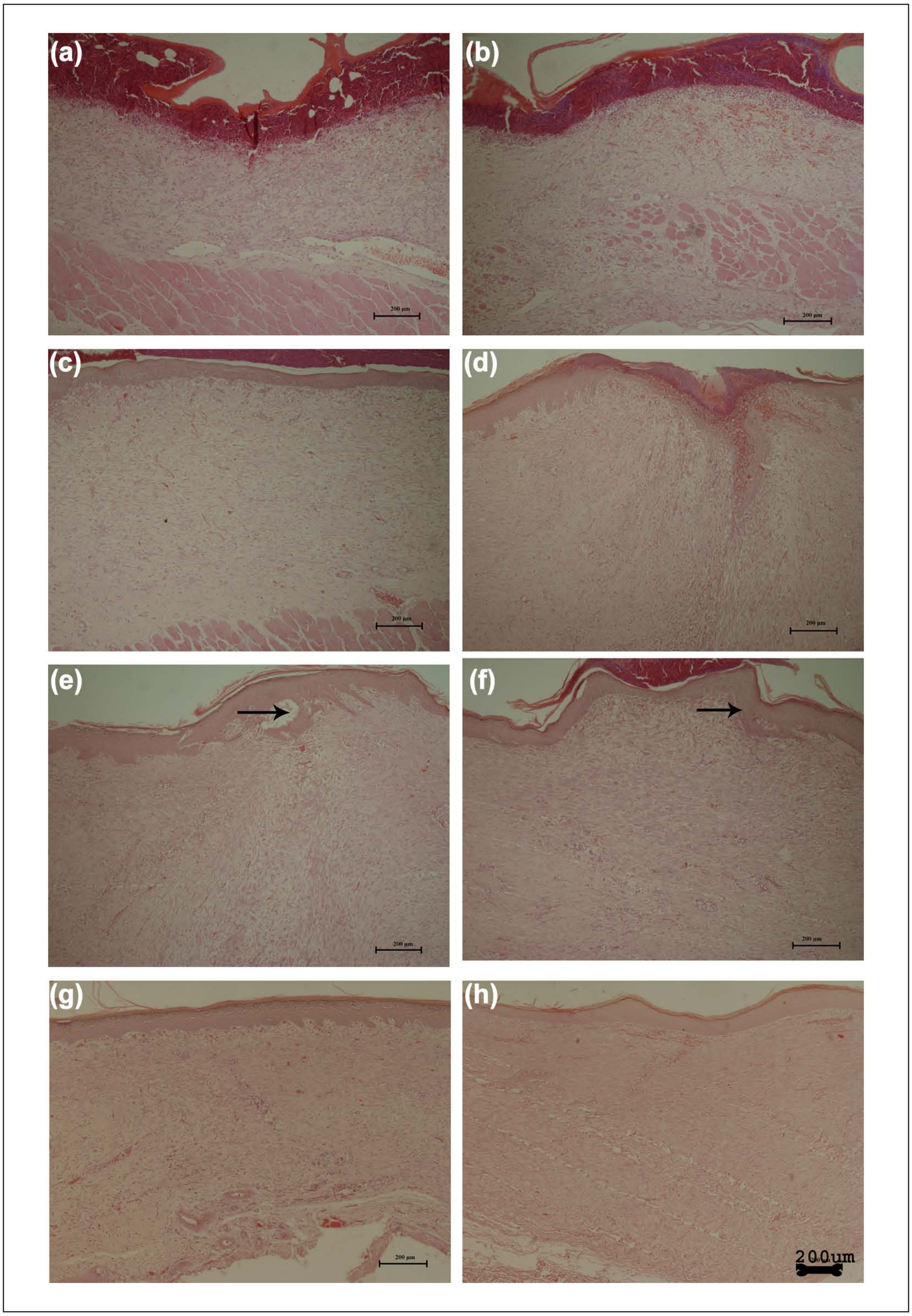

Figure 3. Haematoxylin and eosin staining of (a, c, e and g) CDS-grafted wound and (b, d, f and h) SIS-grafted wound on 3rd, 7th, 14th and 30th day.
CDS: cholecyst-derived scaffold; SIS: small intestinal submucosa.

Pattern of vimentin immunostaining. On the third day (Figure 6(a) and (b)), both CDS and SIS showed heterogeneous distribution of vimentin throughout the wound area, and they appeared like elongated spindles. On the 7th (Figure 6(c) and (d)) and 14th day (Figure 6(e) and (f)), the vimentin content increased showing further scattering and abundance of spindle-shaped cells. In some slides, the density of these cells was higher immediately below the

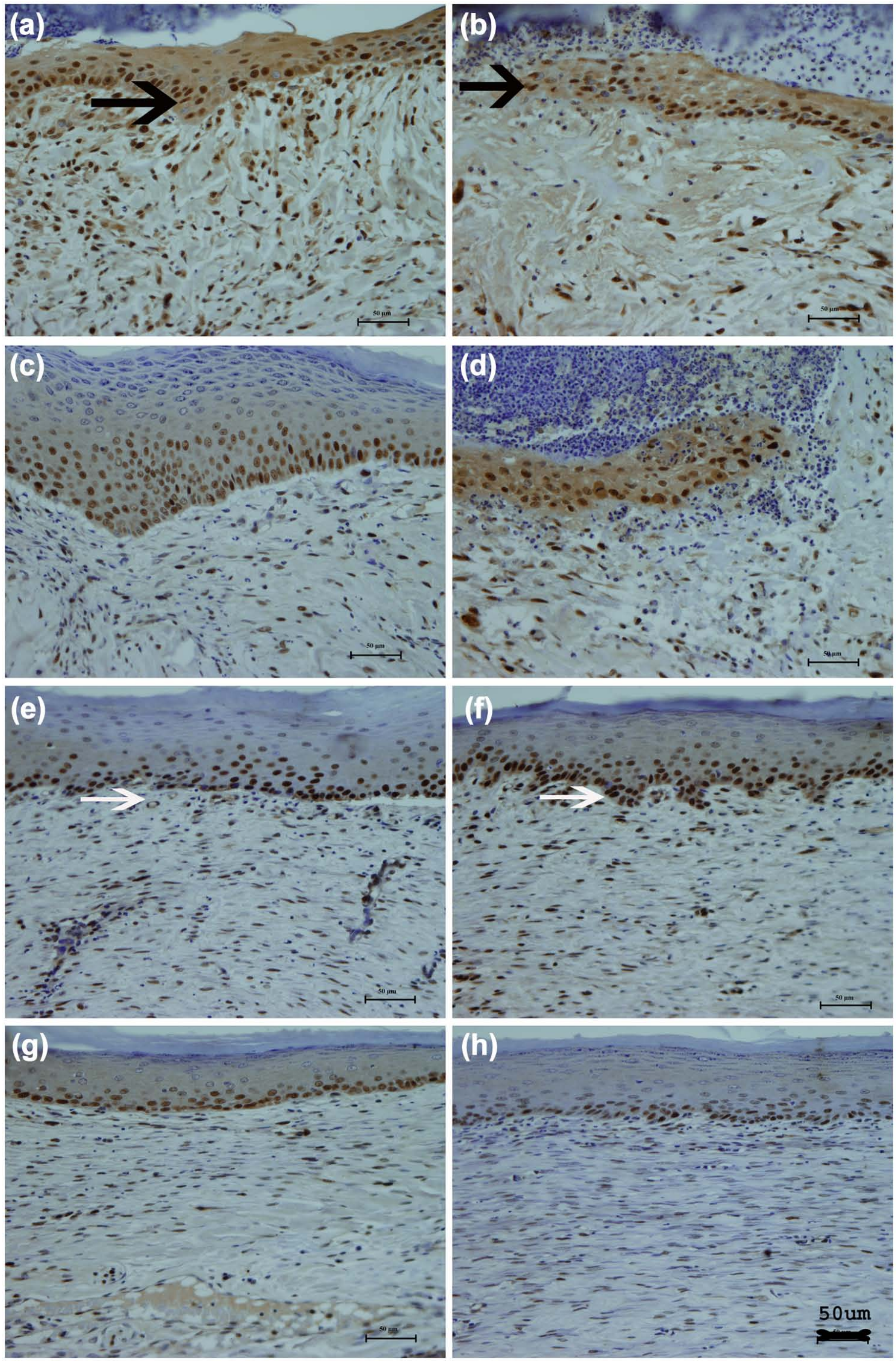

Figure 4. PCNA immuno staining of CDS-grafted wound (a,c,e and g) and SIS-grafted wound (b,d, f and h) on 3rd, 7th, 14th and 30th day. On third day (a and b), most of the basal cells of neo-epidermis (black arrow) and the dermis immediately beneath are positive for PCNA. During 7th day (c and d), the outer layers of epidermis remained negative, but the basal and suprabasal cells in the neo-epidermis show PCNA-positive in both grafts. By 14th (e and f) and 30th day (g and h), only basal cells (white arrow) in epidermis were positive for PCNA. Please see Figure 11(c) for quantitative data.
CDS: cholecyst-derived scaffold; PCNA: proliferating cell nuclear antigen.

neo-epidermis. On the 30th day (Figure 6(g) and (h)), the vimentin proteins were sparse, faint, thin and assumed the shape of an 'elongated wavy thread' like pattern. Both CDS and SIS showed similar pattern in vimentin-positive cells, and there was no significant difference in the vimentin positivity at different time points (Figure 11(d)).

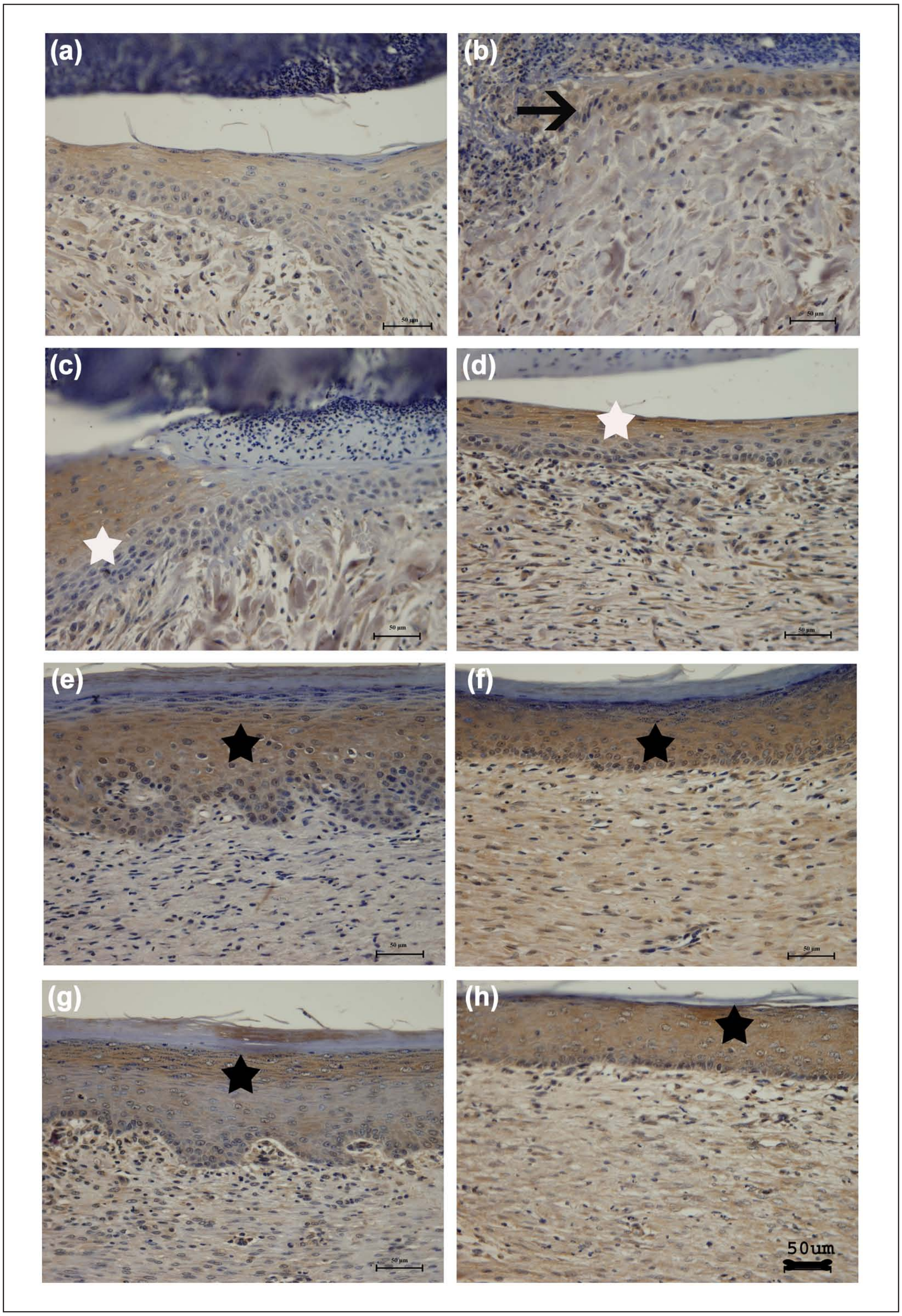

Figure 5. CK-14 immuno staining of CDS-grafted wound (a,c,e and g) and SIS-grafted wound (b,d, f and h) on 3rd, 7th, 14th and 30th day. On 3rd (a and b) and 7th day (c and d), CK-14 deposition can be seen on the leading edge of re-epithelisation (arrow) and the suprabasal keratinocytes of the epidermis (white star) in both CDS- and SIS-grafted wounds. On day 14 (e and f) and day 30 (g and h), the epidermis was completely formed and CK-14 deposition was seen in the middle layers of epidermis (black star) in wounds treated by both the grafts.
CK-14: cytokeratin-14; CDS: cholecyst-derived scaffold; SIS: small intestinal submucosa.

Pattern of alpha-smooth-muscle-actin immunostaining. On the third day (Figure 7(a) and (b)), ASMA-positive cells were seen throughout wound bed. On the seventh day (Figure 7(c) and (d)), their numbers increased and were uniformly distributed all over the healing wound. But by the 14th day (Figure 7(e) and (f)), there were abundant

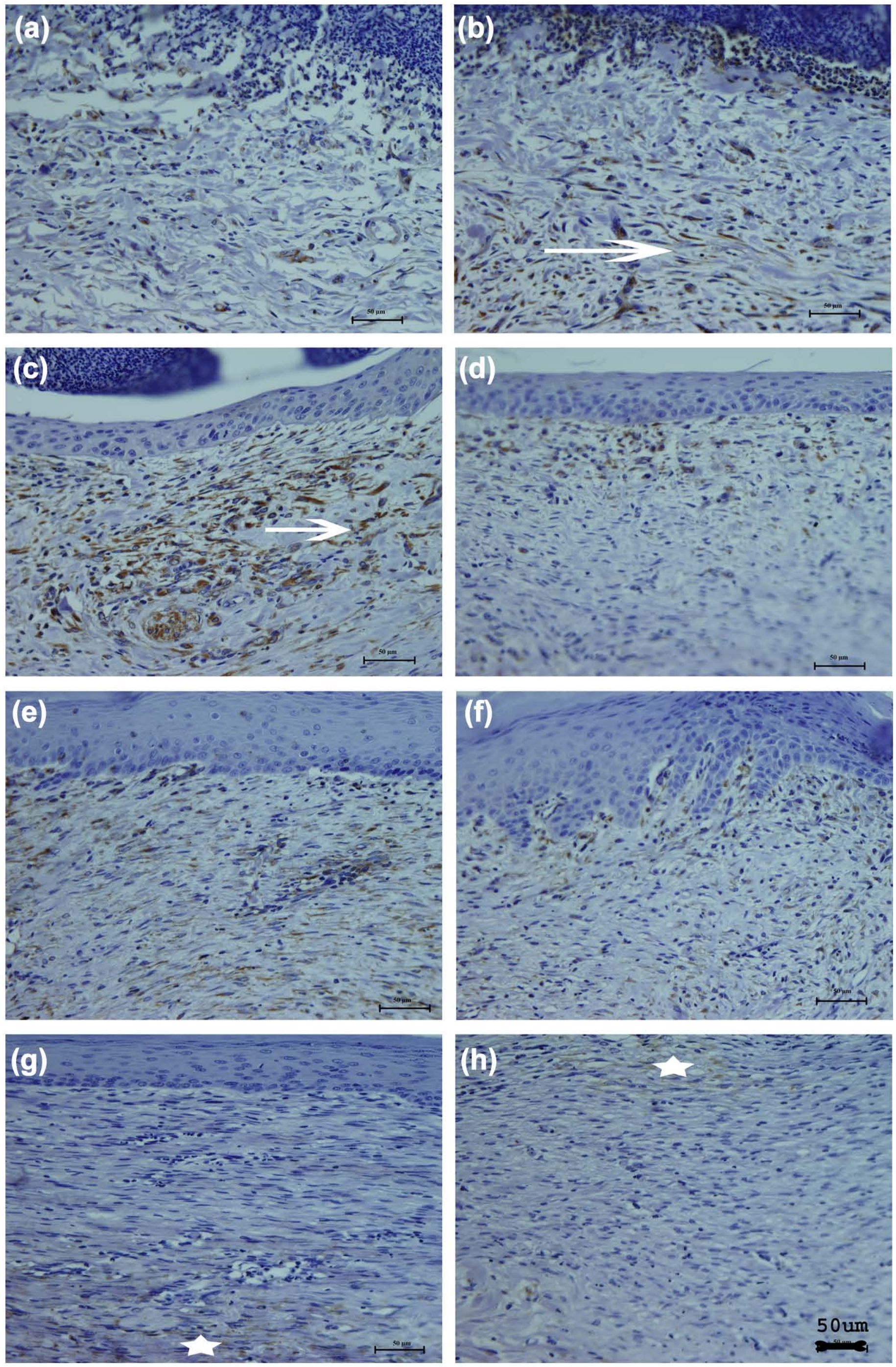

Figure 6. Vimentin immuno staining of CDS-grafted wound (a,c,e and g) and SIS-grafted wound (b,d, f and h) on 3rd, 7th, 14th and 30th day. On third day (a and b), both CDS and SIS showed heterogeneous distribution of vimentin throughout the wound area and they appeared like elongated spindles (star). On 7th (c and d) and 14th day (e and f), the vimentin concentrated below the neo-epidermis showed further elongation and scattering. On 30th day (g and h), vimentin deposition was sparse, faint, thin and assumed the shape of an 'elongated wavy thread' (arrow). Please see Figure 11(d) for quantitative data.
CDS: cholecyst-derived scaffold; SIS: small intestinal submucosa.

ASMA-immunopositive cells immediately below the newly formed neo-epidermis and at the wound–tissue interface in the dermis. On the 30th day (Figure 7(g) and (h)), the density of ASMA-positive cells decreased considerably. There was significantly higher number of these cells with contractile properties in the CDS-grafted wound

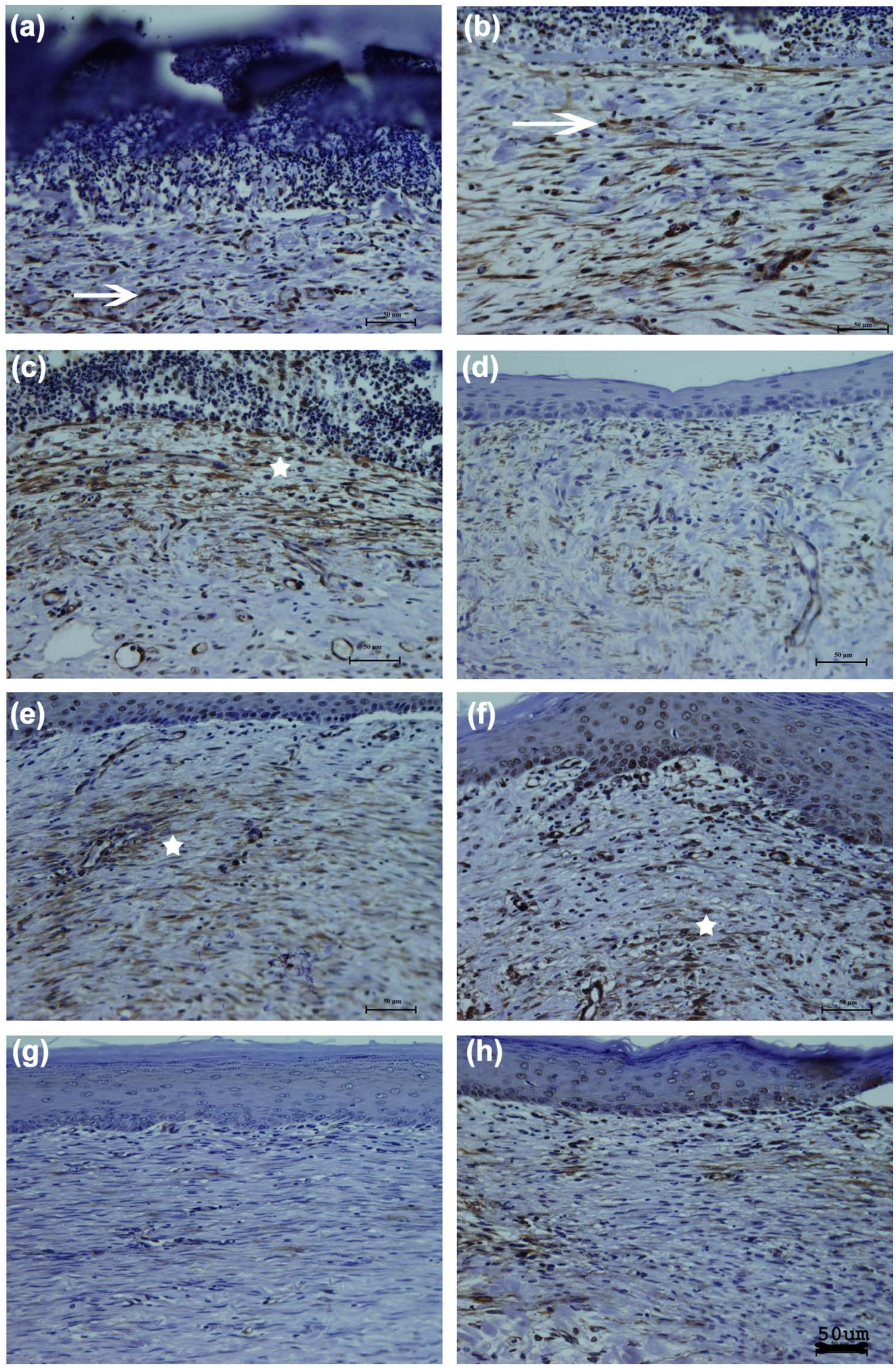

Figure 7. ASMA immuno staining of CDS-grafted wound (a,c,e and g) and SIS-grafted wound (b,d, f and h) on 3rd, 7th, 14th and 30th day. On third day (a and b), ASMA was distributed throughout wound area and showed spindle, elongated and wavy pattern (arrow). On 7th day (c and d) and 14th day (e and f) ASMA further increased (star) and was concentrated below the newly formed epidermis and at the wound–tissue interface in the dermis. During day 30 (g and h), ASMA concentration decreased compared to day 14. Please see Figure 11(e) for quantitative data.
CDS: cholecyst-derived scaffold; SIS: small intestinal submucosa; ASMA: anti-smooth muscle antibody.

(p value = 0.009) during early phases (third day) of wound healing. However, the pattern of ASMA was similar in both CDS and SIS on later time points (Figure 11(e)).

Extent of collagen deposition and remodelling. The extent of collagen deposition also was similar in both CDS and SIS (Figures 8, 9 and 11(f)). There was an increase in the extent of

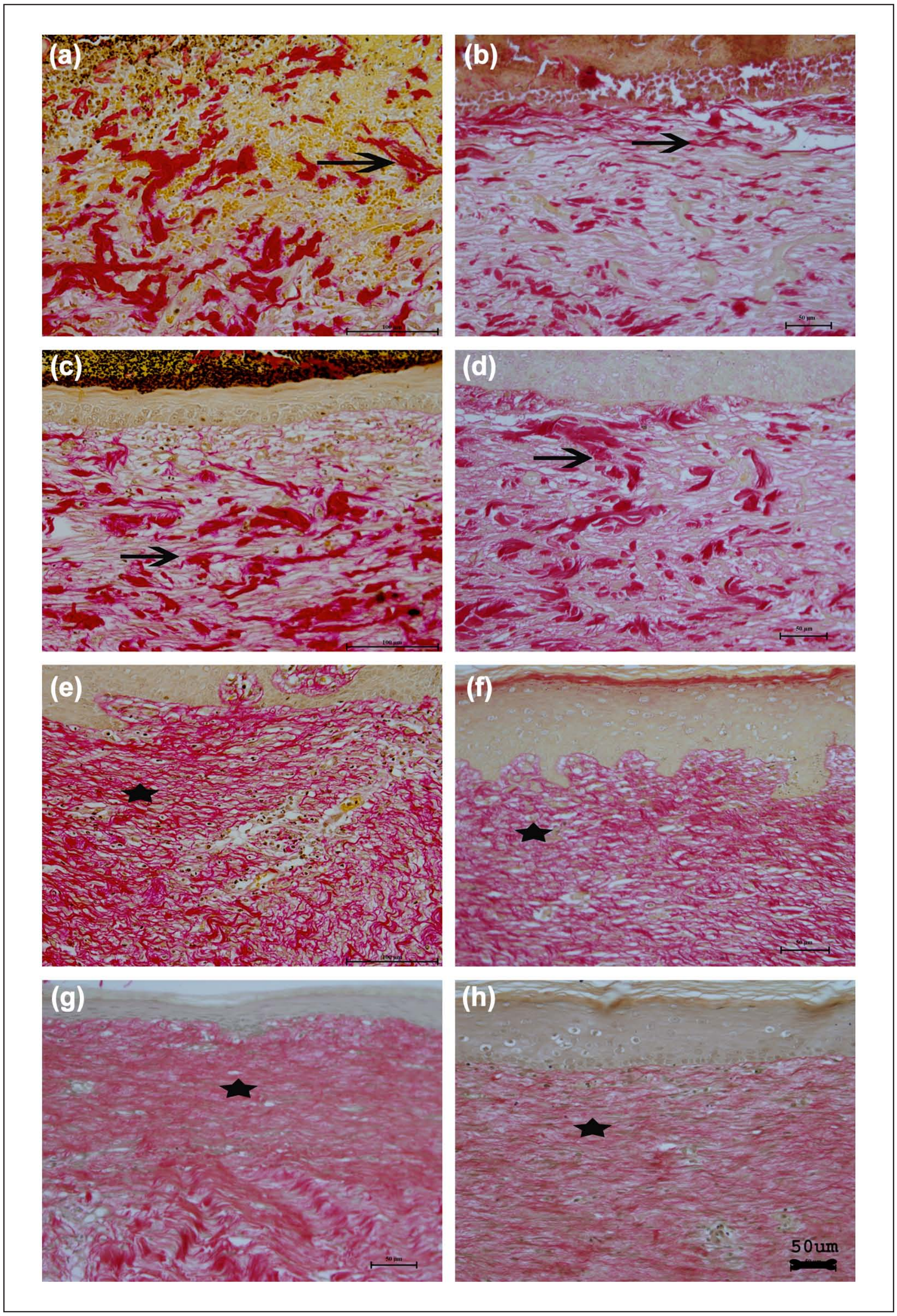

Figure 8. Picro-sirius red staining of (a, c, e and g) CDS-grafted wound and (b, d, f and h) SIS-grafted wound on 3rd, 7th, 14th and 30th day. Collagen deposition increased from 3 to 7 days. On 14th (e and f) and 30th day (g and h), the collagen fibres were elongated and closely arranged (star) than 3rd (a and b) and 7th day (c and d) when collagen fibres are seen as bundles (arrow). Please see Figure 11(f) for quantitative data.
CDS: cholecyst-derived scaffold; SIS: small intestinal submucosa.

collagen deposition by 7 days (about 20%) and 14 days (about 40%) (Figure 11(f)). The ratio of type I to type III was similar during early time period in both grafts, but type I collagen deposition increased during the late time points (Figure 12(a)).

Distribution of elastin in the healing wounds. There was no significant difference in deposition of elastin in both SIS and CDS during 7th day and 30th day (Figures 10 and 12(b)).

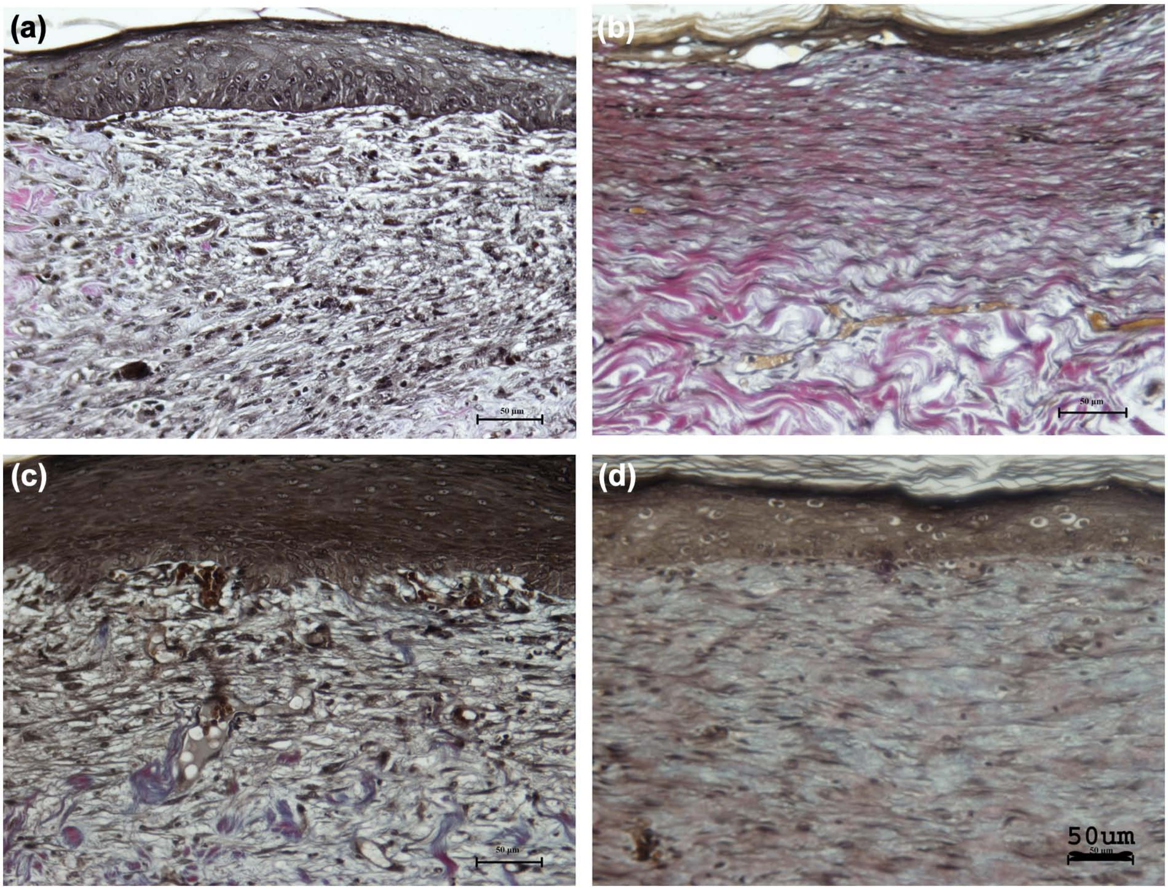

Figure 9. Herovici staining of (a and b) CDS-grafted wound and (c and d) SIS-grafted wound on 7th and 30th day. The CDS-grafted wound showed higher type I collagen deposition (red fibres) on 30 days (b and d) compared to SIS-grafted wounds. Please see Figure 12(a) for quantitative data.
CDS: cholecyst-derived scaffold; SIS: small intestinal submucosa.

Discussion

Extracellular matrices derived from mammalian organs and tissues have wide range of applications in regenerative medicine. Here, we used CDS as a skin graft for treating full-thickness skin wounds in rabbit with the objective of evaluating its potential for promoting healing by regeneration.

The clue for proposing the use of CDS for skin-graft applications originated from its physical and biological properties (Figures 1 and 2) as the biological and physical properties of any scaffold can influence wound healing.[21] Additionally, certain biomarkers that occur at the wound site can also predict the potential of a scaffold for cutaneous wound-healing applications.[24] Here, we studied some of these parameters like elastin and sulphated-GAG content of the scaffold (Figure 2(a)). An important physical parameter often studied for evaluating healing potential is the WVTR from the graft that indicates its ability to retain absorbed water.[25,26] High WVTR rate might cause the wound bed to become desiccated and consequently lead to loss of integrity. It may also modulate various tissue responses in the healing wound, for example, too much water loss increases the possibility of tissue necrosis and slowing of epithelial cell migration leading to impediment of re-epithelisation and decreased oxygen availability for bacterial killing leading to increased risk of infection and impaired nutrient flow.[27] These are all poor prognosis for wound healing. The novel scaffold CDS we selected had lower WVTR compared to the reference scaffold (Figure 1(d)). Adequate moisture is also required for satisfactory activity of growth factors and proteolytic enzymes. Furthermore, moisture also enhances fibroblast/endothelial cell proliferation and is known to increase the immune defence of wound surface.[28] Epithelial cells need a moist ground to migrate and re-epithelise faster.[29] The other hydration parameters such as percentage fluid uptake, moisture content of the graft and EWL of the CDS graft

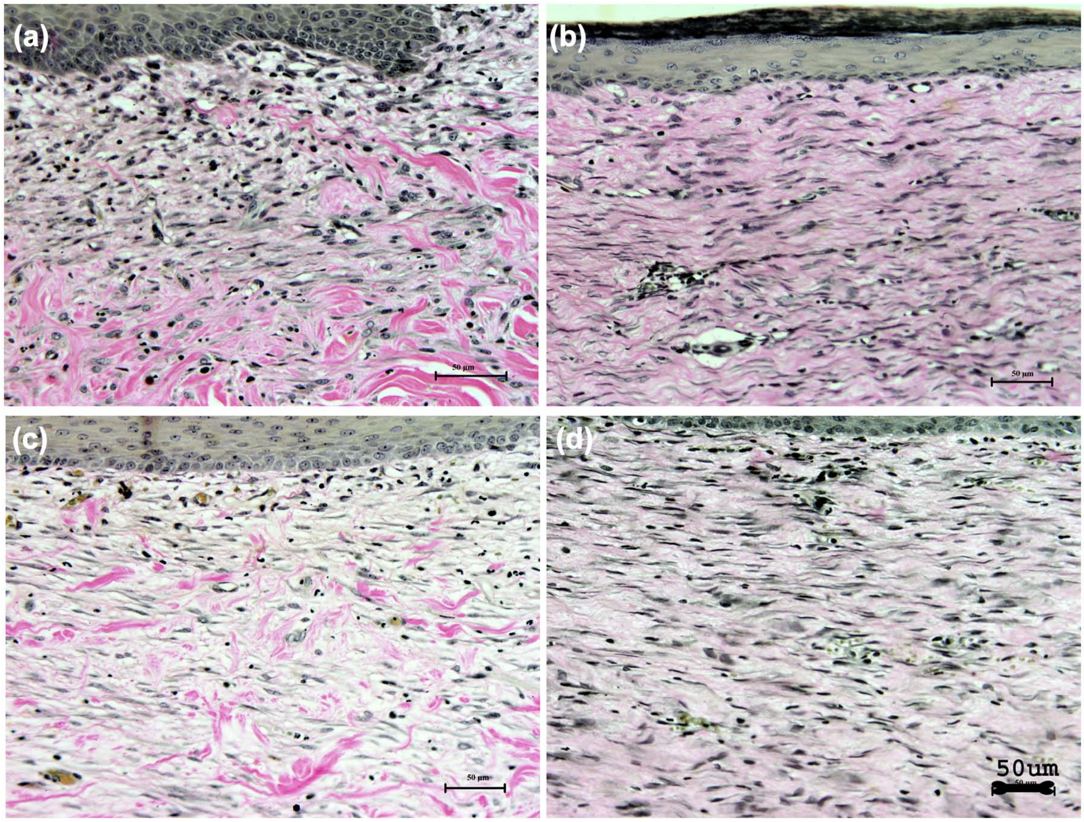

Figure 10. Van Gieson staining of (a and b) CDS-grafted wound and (c and d) SIS-grafted wound on 7th (a and c) and 30th day (b and d). Note that the elastin deposition (black fibres) increased on 30th day (b and d) in both CDS- and SIS-grafted wounds. Please see Figure 12(b) for quantitative data.
CDS: cholecyst-derived scaffold; SIS: small intestinal submucosa.

were similar with that of the commercially available reference graft.

The flexural rigidity and suture retention efficiency are two parameters that indicate the suitability of a scaffold as skin graft and for better wound healing.[21] Flexural rigidity corresponds to the ability of a dressing or graft to drape over the wound. It should be sufficiently low. On the other hand, high flexural rigidity means a rigid scaffold that will not be flexible to be in touch with the wound surface. In the present instance, the flexural rigidity of CDS was similar to that of the reference product (Figure 1(e)). On the other hand, CDS (2.3 ± 9 N) had lower suture retention ability than that of SIS (Figure 1(f)). But the actual measure of the suture efficiency was higher than 1.2 N as expected for scaffold sheets commonly used in soft tissue engineering applications.[30] Hence, CDS can be considered for skin-graft applications.

The CDS had higher content of macromolecules like elastin and sulphated GAGs than SIS while the collagen content was similar (Figure 2(a)). It was not sure whether the higher elastin and sulphated-GAG content reflected the natural content of these molecules in normal for CDS and whether the processing and extraction techniques have affected the values observed. Nevertheless, higher content of these biomolecules in CDS made it a better scaffold than SIS for skin-graft application. It is known that elastin enhances angiogenesis,[31] promotes proliferation of endothelial cells[32] and also supports proliferation of dermal fibroblasts.[33] The GAGs facilitate specific interactions to cytokines[34] and chemotactic growth factors[35] which are important for wound healing as they can regulate the release of growth factors in the healing environment. In addition, GAGs can also trap water in the form of gel and prevent loss of water. This corroborated the observations made about WVTR in CDS (Figure 1(d)) as discussed earlier.

The presence of excess cellular content, especially nucleic acids, in a scaffold is known to cause inflammatory reactions that are not congenial for a good scaffold.[36] In the present instance, however, the CDS scaffold had contained lower DNA content compared to SIS (Figure 2(b)). This is probably because gall bladder is not a very cellular organ since its main function is storage and release of bile, unlike the small intestine which

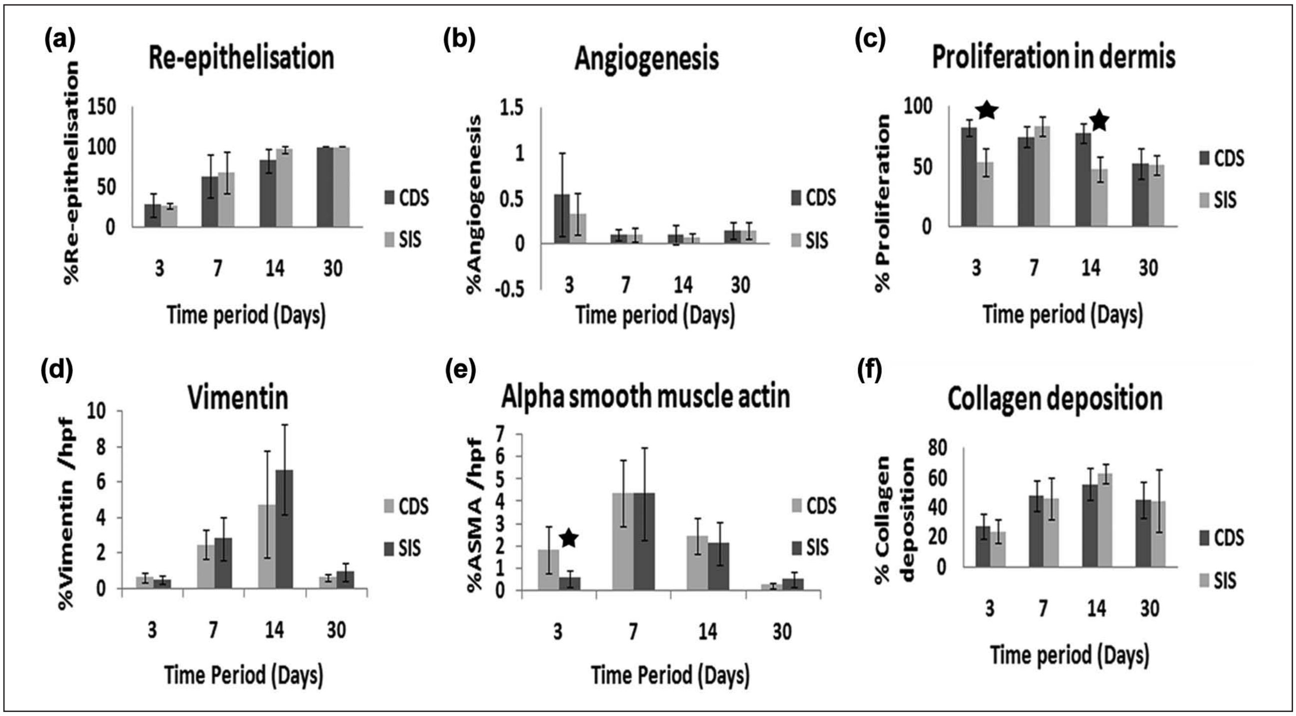

Figure 11. Quantitative histomorphometry for early stage wound-healing parameters: (a) percentage re-epithelisation, (b) angiogenesis, (c) cell proliferation in dermis, (d) area occupied by vimentin-positive cells, (e) area occupied by alpha smooth muscle actin positive cells and (f) collagen deposition. The CDS-grafted wound showed higher ASMA-positive area on 3rd day (p value = 0.009) as well as cell proliferation on 3rd (p value = 0.02) and 14th day (p value = 0.008).
CDS: cholecyst-derived scaffold; ASMA: anti-smooth muscle antibody.

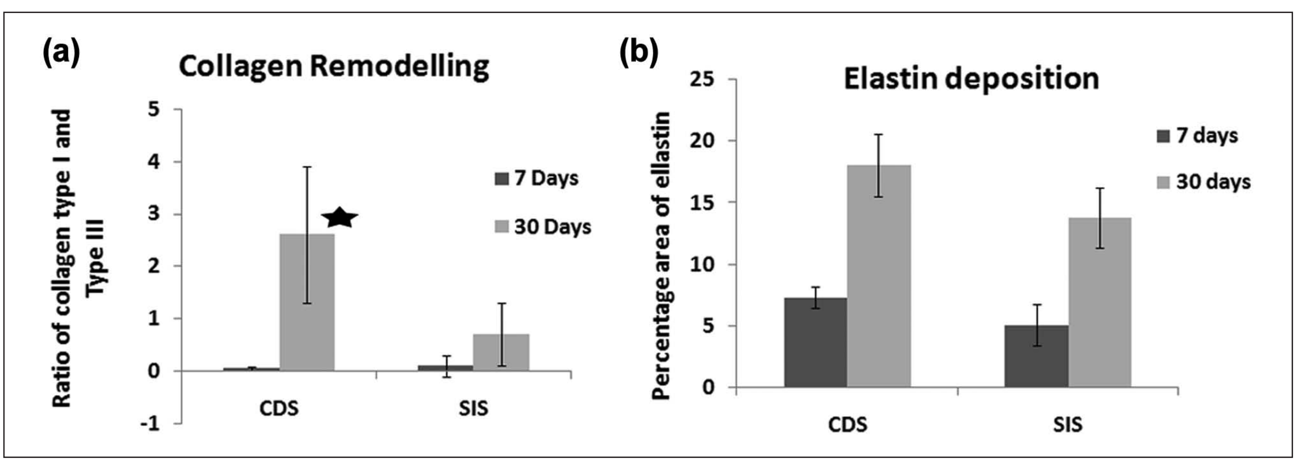

Figure 12. Quantitative data for late-stage wound-healing parameters: (a) ratio of collagen type I to collagen type III ratio, (b) elastin deposition. CDS had higher type 1 to type III collagen ratio compared to SIS on 30th day (p value = 0.005).
CDS: cholecyst-derived scaffold; SIS: small intestinal submucosa.

is involved in digestion, peristalsis and secretion with wide absorptive surface organised into primary and secondary folding. Thus, compared to the reference material, the higher content of sulphated GAGs (Figure 2(a)) as well as elastin (Figure 2(a)) and lower content of DNA (Figure 2(b)) in CDS make it a preferred biomaterial for graft-assisted healing.

To investigate the wound-healing potential of CDS in a preclinical setting, we grafted full-thickness skin wound in a rabbit model as in earlier studies.[37] The healing reaction was assessed by histomorphology and compared with those caused by a clinically proven graft material (Figures 3–10). The histomorphology observations were cross-verified with histomorphometry data (Figures 11 and 12). The quantitative data on re-epithelisation (Figure 11(a)), angiogenesis pattern (Figure 11(b)), cell proliferation (Figure 11(c)), the distribution of vimentin-positive mesenchymal cells (Figure 11(d)), the distribution of ASMA-positive myofibroblasts (Figure 11(e)) and the extent of collagen deposition (Figure 11(f)) provided objective evidence on the differential healing ability of CDS graft compared to a commercial graft. The data on cell proliferation (Figures 4 and 11(c)) indicated healing by regeneration in the early phase (up to 14 days) of the healing and later achieving a balanced and equilibrated remodelling phase reaction (by 30 days) with that of the reference scaffold.

The distribution of CK-14 positive epidermal cells (Figure 5) was evaluated by IHC for studying the wound-closure ability and the distribution of newly formed keratinocytes in the neo-epidermis, as suggested by existing literature.[38] It is known that CK-14, expressed in dividing basal keratinocytes, helps in maintaining epidermal cell shape, provides resistance to mechanical stress and acts as negative regulator of terminal differentiation of keratinocytes.[39] Both the grafts showed initiation of wound closure by third day as evident from CK-14 positivity (Figure 5(a) and (b)) at the leading edge of the neodermis formed over the wound. As most of the suprabasal keratinocytes of the epidermis were positive for CK-14 during seventh day (Figure 5(c) and (d)), it was concluded that terminal differentiation of keratinocytes and their migration were happening only by the seventh day in both the scaffold-treated wounds. On the other hand, by the 14th and the 30th day, the CK-14 deposition was seen in mid-epidermis, which indicated completion of wound closure and completion of re-epithelisation process in both graft–treated wounds (Figure 5(e)–(h)). Significantly, the proliferation of epidermal cells was higher in the epidermis (Figure 11(c)) in the CDS-treated wound compared to SIS-treated wound in the proliferation phase (3 days) and early remodelling phase (14 days). However, at the end of the healing process (30 days), as desired, there was no significant difference. The abundance of proliferating cells in dermis was evaluated by IHC for PCNA (Figure 4). Higher rates of proliferation and cell turnover were observed in CDS compared to SIS during the initial (third day) phase of healing (Figure 11(c)), and this suggested that CDS stimulated regeneration of cells, presumably those cells involved in better wound healing. Similarly, the cell turnover at the later remodelling phases of wound healing (14th day) was also higher in the CDS-grafted wound, suggesting their active participation in the remodelling process. The contributory roles of some of the important cell types, especially epithelial (keratinocyte) and mesenchymal (fibroblast), were apparent when studied objectively by quantitative methods.

During the initial stages of the wound healing, fibroblasts from the surrounding normal area are known to migrate and proliferate into the wound site and within 3–4 days get converted to myofibroblasts.[40] The main function of myofibroblasts in a healing wound is contraction by synthesising of ECM proteins, notably, collagen types I–VI and XVIII, laminin, thrombospondin, glycoproteins and proteoglycans for the dermal repair. The myofibroblasts usually go on increasing from the inflammatory stage (3–4 days) till the end of proliferation phase (14–15 days), and by the remodelling phase (around 21–30 days), these myofibroblasts undergo apoptosis[41] and ASMA in fibroblasts regulate the proteins responsible for motility and contractility.[42] To know the nature of this regulation, we quantified the extent of ASMA immunoreactivity in tissue section (Figure 7) and accessed the nature of wound contraction. The presence of ASMA was highest during 14th day in both the groups and then decreased thereafter, which was in accordance with previous literature.[43] However, there was significant increase in the ASMA-positivity during the initial inflammatory stage of healing in CDS scaffold compared to SIS (Figure 11(e)). This suggested that CDS scaffold can bring about more organised healing through better wound contraction and deposition of ECM. It is remarkable to note that there has not been any excess collagen deposition at any stage, and the remodelling induced by CDS and SIS was similar at 14 and 30 days.

In normal healthy human skin, the type I/type III collagen ratio is 3.5:1. In hypertrophic scarring, the ratio may become 2:1 as the amount of type III is higher.[44] The type I to type III collagen ratio in CDS (2.6 ± 1.8:1) after 30 days was near to that of normal skin than that of the SIS-induced healing reaction (0.7 ± 0.7:1, Figure 12(a)). During the onset of healing, the proliferating fibroblast starts to synthesise collagen, and the total collagen content increases preferentially with excess of collagen type III over type I. Hence, in the healing, reaction with respect to collagen deposition (Figures 8 and 12(a)) was assumed normal. However, type I collagen is ultimately responsible for the tensile strength, continuity and function of skin. As remodelling and maturation occurs, the type III collagen is expected to decrease in comparison with type I collagen, trying to revert back to normal skin.[45] Moreover, decrease in type I collagen and an increase in type III collagen are associated with thinner and more flexible collagen fibres leading to reduction in tensile strength.[46] In this study, there is significant increase in type I collagen (Figure 12(a)) in CDS-grafted wound in 30 days compared to the SIS-grafted wound. This implied that the tensile strength in CDS-grafted skin was higher than SIS. However, the elastin deposition in both CDS and SIS showed similar increase from 7 to 30 days of healing (Figure 12(b)), indicating uncomplicated wound contraction.

Thus, the nature of cell proliferation, infiltration and collagen deposition indicated that the healing pattern induced by CDS was different from that caused by SIS. The former caused enhanced cell proliferation at the regenerative phase (early stage). There was excess collagen-I deposition that enhanced tensile strength but without significant difference in elastin.

Conclusion

The potential of ECM scaffold isolated from cholecyst was evaluated in vitro and in vivo for use as skin graft. The results indicated that ECM scaffold isolated from cholecyst is a satisfactory skin graft for wound-healing applications. The CDS promoted a prominent healing reaction with enhanced cell proliferation and adequate collagen deposition.

Acknowledgements

Ms Deepa is a Senior Research Fellow (SRF) of the CSIR. The authors thank Mr NK Thulaseedharan and CS Geetha for technical support.

Declaration of conflicting interests

The authors declared no potential conflicts of interest with respect to the research, authorship and publication of this article.

Funding

The work was supported by the Department of Biotechnology, Government of India [BT/PR15461/MED/32/167/2011]

References

1. Cronin H and Goldstein G. Biologic skin substitutes and their applications in dermatology. *Dermatol Surg* 2013; 39: 30–34.
2. Pereira C, Gold W and Herndon D. Review paper: burn coverage technologies: current concepts and future directions. *J Biomater Appl* 2007; 22: 101–121.
3. Daley WP, Peters SB and Larsen M. Extracellular matrix dynamics in development and regenerative medicine. *J Cell Sci* 2008; 121: 255–264.
4. Reing JE, Zhang L, Myers-Irvin J, et al. Degradation products of extracellular matrix affect cell migration and proliferation. *Tissue Eng Pt A* 2009; 15: 605–614.
5. Kleinman HK, Philp D and Hoffman MP. Role of the extracellular matrix in morphogenesis. *Curr Opin Biotech* 2003; 14: 526–532.
6. Raines EW. The extracellular matrix can regulate vascular cell migration, proliferation, and survival: relationships to vascular disease. *Int J Exp Pathol* 2000; 81: 173–182.
7. Badylak SF, Freytes DO and Gilbert TW. Extracellular matrix as a biological scaffold material: structure and function. *Acta Biomater* 2009; 5: 1–13.
8. Mostow EN, Haraway GD, Dalsing M, et al. Effectiveness of an extracellular matrix graft (OASIS Wound Matrix) in the treatment of chronic leg ulcers: a randomized clinical trial. *J Vasc Surg* 2005; 41: 837–843.
9. Kim MS, Hong KD, Shin HW, et al. Preparation of porcine small intestinal submucosa sponge and their application as a wound dressing in full-thickness skin defect of rat. *Int J Biol Macromol* 2005; 36: 54–60.
10. Schallberger SP, Stanley BJ, Hauptman JG, et al. Effect of porcine small intestinal submucosa on acute full-thickness wounds in dogs. *Vet Surg* 2008; 37: 515–524.
11. Zheng MH, Chen J, Kirilak Y, et al. Porcine small intestine submucosa (SIS) is not an acellular collagenous matrix and contains porcine DNA: possible implications in human implantation. *J Biomed Mater Res B Appl Biomater* 2005; 73: 61–67.
12. John TT, Aggarwal N, Singla AK, et al. Intense inflammatory reaction with porcine small intestine submucosa pubovaginal sling or tape for stress urinary incontinence. *Urology* 2008; 72: 1036–1039.
13. Burugapalli K, Thapasimuttu A, Chan JC, et al. Scaffold with a natural mesh-like architecture: isolation, structural, and in vitro characterization. *Biomacromolecules* 2007; 8: 928–936.
14. Burugapalli K, Chan JCY, Kelly JL, et al. Buttressing staples with cholecyst-derived extracellular matrix (CEM) reinforces staple lines in an ex vivo peristaltic inflation model. *Obes Surg* 2008; 18: 1418–1423.
15. Brody S, McMahon J, Yao L, et al. The effect of cholecyst-derived extracellular matrix on the phenotypic behaviour of valvular endothelial and valvular interstitial cells. *Biomaterials* 2007; 28: 1461–1469.
16. Coburn JC, Brody S, Billiar KL, et al. Biaxial mechanical evaluation of cholecyst-derived extracellular matrix: a weakly anisotropic potential tissue engineered biomaterial. *J Biomed Mater Res A* 2007; 81: 250–256.
17. Burugapalli K and Pandit A. Characterization of tissue response and in vivo degradation of cholecyst-derived extracellular matrix. *Biomacromolecules* 2007; 8: 3439–3451.
18. Chan JCY, Burugapalli K, Naik H, et al. Amine functionalization of cholecyst-derived extracellular matrix with generation 1 PAMAM dendrimer. *Biomacromolecules* 2008; 9: 528–536.
19. Burugapalli K, Chan JCY, Naik H, et al. Tailoring the properties of cholecyst-derived extracellular matrix using carbodiimide cross-linking. *J Biomat Sci-Polym E* 2009; 20: 1049–1063.
20. Pandima Devi M, Sastry TP and Meignanalakshmi S. Preparation and characterization of fibrin-chitosan composite and its in vivo studies. *J Pharmacy* 2012; 2(6): 21–32.
21. Yannas IV and Burke JF. Design of an artificial skin. I. Basic design principles. *J Biomed Mater Res* 1980; 14: 65–81.
22. Muhamed J, Revi D, Joseph R, et al. Phenotypic modulation of cell types around implanted polyethylene terephthalate fabric in rabbit muscle. *Toxicol Pathol* 2013; 41: 497–507.
23. Lillie RD, Tracy RE, Pizzolato P, et al. Differential staining of collagen types in paraffin sections: a color change in degraded forms. *Virchows Arch A Pathol Anat Histol* 1980; 386: 153–159.
24. Hahm G, Glaser JJ and Elster EA. Biomarkers to predict wound healing: the future of complex war wound management. *Plast Reconstr Surg* 2011; 127(Suppl. 1): 21S–26S.
25. Palamand S, Reed AM and Weimann LJ. Testing intelligent wound dressings. *J Biomater Appl* 1992; 6: 198–215.

26. Vatankhah E, Prabhakaran MP, Jin G, et al. Development of nanofibrous cellulose acetate/gelatin skin substitutes for variety wound treatment applications. *J Biomater Appl* 2013; 2: 1–10.
27. Chang H, Wind S and Kerstein MD. Moist wound healing. *Dermatol Nurs* 1996; 8: 174–176.
28. Bryan J. Moist wound healing: a concept that changed our practice. *J Wound Care* 2004; 13: 227–228.
29. Szycher M and Lee SJ. Modern wound dressings: a systematic approach to wound healing. *J Biomater Appl* 1992; 7: 142–213.
30. Tran RT, Thevenot P, Zhang Y, et al. Scaffold sheet design strategy for soft tissue engineering. *Nat Mater* 2010; 3: 1375–1389.
31. Robinet A, Fahem A, Cauchard JH, et al. Elastin-derived peptides enhance angiogenesis by promoting endothelial cell migration and tubulogenesis through upregulation of MT1-MMP. *J Cell Sci* 2005; 118: 343–356.
32. Long MM, King VJ, Prasad KU, et al. Elastin repeat peptides as chemoattractants for bovine aortic endothelial-cells. *J Cell Physiol* 1989; 140: 512–518.
33. Rnjak J, Li Z, Maitz PKM, et al. Primary human dermal fibroblast interactions with open weave three-dimensional scaffolds prepared from synthetic human elastin. *Biomaterials* 2009; 30: 6469–6477.
34. Coombe DR. Biological implications of glycosaminoglycan interactions with haemopoietic cytokines. *Immunol Cell Biol* 2008; 86: 598–607.
35. Kirker KR, Luo Y, Nielson JH, et al. Glycosaminoglycan hydrogel films as bio-interactive dressings for wound healing. *Biomaterials* 2002; 23: 3661–3671.
36. Keane TJ, Londono R, Turner NJ, et al. Consequences of ineffective decellularization of biologic scaffolds on the host response. *Biomaterials* 2012; 33: 1771–1781.
37. Revi D, Paul W, Anilkumar T, et al. Differential healing of full thickness rabbit skin wound by fibroblast loaded chitosan sponge. *J Biomater Tissue Eng* 2013; 3(3): 261–272.
38. Braiman-Wiksman L, Solomonik I, Spira R, et al. Novel insights into wound healing sequence of events. *Toxicol Pathol* 2007; 35: 767–779.
39. Alam H, Sehgal L, Kundu ST, et al. Novel function of keratins 5 and 14 in proliferation and differentiation of stratified epithelial cells. *Mol Biol Cell* 2011; 22: 4068–4078.
40. Klingberg F, Hinz B and White ES. The myofibroblast matrix: implications for tissue repair and fibrosis. *J Pathol* 2013; 229: 298–309.
41. Li B and Wang JHC. Fibroblasts and myofibroblasts in wound healing: force generation and measurement. *J Tissue Viability* 2011; 20: 108–120.
42. Hinz B, Celetta G, Tomasek JJ, et al. Alpha-smooth muscle actin expression upregulates fibroblast contractile activity. *Mol Biol Cell* 2001; 12: 2730–2741.
43. Desmoulière A, Chaponnier C and Gabbiani G. Tissue repair, contraction, and the myofibroblast. *Wound Repair Regen* 2005; 13: 7–12.
44. Widgerow AD, Chait LA, Stals R, et al. New innovations in scar management. *Aesthet Plast Surg* 2000; 24: 227–234.
45. Cheng W, Yan-Hua R, Fang-Gang N, et al. The content and ratio of type I and III collagen in skin differ with age and injury. *Afr J Biotechnol* 2011; 10: 2524–2529.
46. Eriksen HA, Pajala A, Leppilahti J, et al. Increased content of type III collagen at the rupture site of human Achilles tendon. *J Orthopaed Res* 2002; 20: 1352–1357.